J. Korean Earth Sci. Soc., v. 40, no. 4, p. 392–405, August 2019
https://doi.org/10.5467/JKESS.2019.40.4.392
ISSN 1225-6692 (printed edition)
ISSN 2287-4518 (electronic edition)

Impacts of Albedo and Wind Stress Changes due to Phytoplankton on Ocean Temperature in a Coupled Global Ocean-biogeochemistry Model

Hyun-Chae Jung[1,2] and Byung-Kwon Moon[1,*]

[1]Division of Science Education and Institute of Fusion Science, Chonbuk National University, Jeonju 54896, Korea
[2]Mirae Climate Co., Ltd., Seoul 08511, Korea

Abstract: Biogeochemical processes play an important role in ocean environments and can affect the entire Earth's climate system. Using an ocean-biogeochemistry model (NEMO-TOPAZ), we investigated the effects of changes in albedo and wind stress caused by phytoplankton in the equatorial Pacific. The simulated ocean temperature showed a slight decrease when the solar reflectance of the regions where phytoplankton were present increased. Phytoplankton also decreased the El Niño-Southern Oscillation (ENSO) amplitude by decreasing the influence of trade winds due to their biological enhancement of upper-ocean turbulent viscosity. Consequently, the cold sea surface temperature bias in the equatorial Pacific and overestimation of the ENSO amplitude were slightly reduced in our model simulations. Further sensitivity tests suggested the necessity of improving the phytoplankton-related equation and optimal coefficients. Our results highlight the effects of altered albedo and wind stress due to phytoplankton on the climate system.

Keywords: ocean biogeochemical processes, ocean-biogeochemistry model, wind stress, albedo, NEMO-TOPAZ

1. Introduction

Ocean biogeochemical processes are important components in the Earth's system as they affect the climate system and physical ocean environment (Sathyendranath et al., 1991; Hense et al., 2017; Lim et al., 2017; Park et al., 2019). Phytoplankton is at the center of the biological cycle within the ocean biogeochemical processes. It is distributed broadly throughout the global ocean including near sea ice in the polar areas. The phytoplankton concentration in the equatorial Pacific changes rapidly according to the phases of El Niño-Southern Oscillation (ENSO) since the upwelling brings nutrients to surface from the depth (Park et al., 2011). The impact of climate change on phytoplankton, such as changes in ENSO due to chlorophyll in the equatorial regions have already been identified (Park et al., 2011; Park et al., 2014; Park et al., 2018). In particular, Park et al. (2017) reported that chlorophyll photosynthesis in the equatorial Pacific strengths El Niño amplitude, resulting in the amplification and higher skewness of ENSO. Moreover, Park et al. (2015) identified that phytoplankton in the North Pole region has further exacerbated arctic warming due to positive feedback between phytoplankton, sea ice and shortwave radiation. Given their role in reducing atmospheric carbon dioxide (CO_2) (Arrigo et al., 1999), ocean phytoplankton is an important element in the climate system.

Among the various species of phytoplankton present in the ocean, cyanobacteria, which have positive buoyancy and frequently cause blooming, increase the light absorption and ocean surface albedo as well as reduce the transfer of wind momentum into the ocean (Kahru et al., 1993; Hutchinson and Webster, 1994). Such changes would ultimately induce various feedback processes. Note that cyanobacteria can survive in high ocean temperature (~34°C) (LaRoche and Breitbarth, 2005) and higher temperature favors its growth (Stal, 2009). Thus, these feedbacks would engender favorable physical ocean environment to be more for cyanobacteria

*Corresponding author: moonbk@jbnu.ac.kr
Tel: +82-63-270-2824

growth, thereby contributing to the formation of phytoplankton mat, in other words, phytoplankton community (Sonntag and Hense, 2011).

Recently, these feedbacks were studied by single-column or idealized physical ocean models (Burchard et al., 2006; Sonntag and Hense, 2011; Sonntag, 2013). However, studies applying these feedback processes to a global ocean model have not been reported. Herein, a newly coupled global ocean biogeochemistry model (NEMO-TOPAZ) (Jung, 2019) is used to analyze the effects of the cyanobacteria. To study the changes in the ocean albedo and wind stress caused by the cyanobacteria mats, the equations developed by Sonntag (2013) are presented and the maximum concentration is adjusted to correspond to the model. Moreover, the effects of related processes on the ocean temperature, focusing on the equatorial Pacific region, are examined by a long-term integration of the model.

2. Experimental Setup

2.1. Albedo and wind stress equations

TOPAZ largely separates phytoplankton into diatoms, non-diatom, small cyanobacteria, and diazotroph (Dunne et al., 2012). The processes associated with changes in albedo and wind stress were added to the model, based on small cyanobacteria estimated by TOPAZ, via the feedback equations developed by Sonntag (2013). The ocean surface albedo, α, is calculated at a time, t, as follows:

$$\alpha(t) = \alpha_{phys}(t) + \alpha_{bio}(t)$$
$$\text{with } \alpha_{bio}(t) = \min[\alpha_{bio}^{\max}, \beta C(z=0,t)] \quad (1)$$

where $\alpha_{phys}(t)$ represents the ocean surface albedo calculated in the physical model, $\alpha_{bio}(t)$ represents the ocean surface albedo due to the cyanobacteria, $\alpha_{bio}^{\max}$=0.02, which represents the maximum ocean surface albedo value increased by the cyanobacteria mat (Kahru et al., 1993), and $C(z=0,t)$ represents the surface cyanobacteria concentration estimated in the model. According to Sonntag (2013), the maximum concentration at which cyanobacteria have a maximum impact on the ocean surface is, 10 mmol N m^{-3}, while β that establishes $\alpha_{bio}^{\max} = \beta \cdot 10$ mmol N m^{-3}=0.02 was set to 0.002 m^3 (mmol N m)$^{-1}$ (at concentrations above the maximum concentration, 0.02 is commonly applied as $\alpha_{bio}^{\max}$). However, because this value was defined by observations, there is a large difference in comparison to cyanobacteria estimated by NEMO-TOPAZ, which calculates β by low-resolution monthly fields. Therefore, the maximum concentration of cyanobacteria was calculated by using results from 1948 to 2009 that simulated by NEMO-TOPAZ using CORE-II forcing data (Large and Yeager, 2009). In other words, the maximum concentration was set to 0.477 mmol N m^{-3}, which corresponds to the average of the top 25% small cyanobacteria concentrations estimated over 62 years. Accordingly, β that establishes $\alpha_{bio}^{\max} = \beta \cdot 0.477$ mmol N m^{-3}=0.02 was set to 0.042 m^3 (mmol N m)$^{-1}$.

Similarly, equation (2) defines the changes in the surface wind stress $\vec{\tau}(t)$ based on the surface cyanobacteria concentration, $C(z=0,t)$.

$$\vec{\tau}(t) = \vec{\tau}_{phys}(t) r_{bio}(t)$$
$$\text{with } r_{bio}(t) = \max[r_{bio}^{\max}, (1 - \delta C(z=0,t))] \quad (2)$$

where $\vec{\tau}_{phys}(t)$ is the wind stress from the atmospheric wind, and $r_{bio}(t)$ is the rate of change in wind stress due to cyanobacteria. $r_{bio}^{\max}$, which represents the rate of change in maximum stress obtained from the observations reported by Deacon (1979), was set to 0.33. Based on $r_{bio}^{\max}$ and the previously determined mat concentration by NEMO-TOPAZ ($r_{bio}^{\max} = 1 - \delta \cdot 0.477$ mmol N m^{-3}=0.33), the constant δ was set to 1.405 m^3 (mmol N m)$^{-1}$.

2.2. Model setup and data

The physical initial and boundary conditions for NEMO-TOPAZ used NEMO reference configurations inputs version 3.6, provided by the NEMO Consortium (https://github.com/NEMO-consortium). The biogeochemical initial and boundary conditions are from Australian Research Council's Centre of Excellence for Climate System Science (ARCCSS, 2018). The

Table 1. Summary of experiments for F-exp set

Experiment name	Biological feedback component	Equation or parameter
Control		$\alpha_{bio}=0$ of (1) and $r_{bio}=0$ of (2)
Alb	Albedo	(1)
Tau	Wind stress	(2)
Alb+Tau	Albedo and wind stress	(1) and (2)

Table 2. Constant values used in the sensitivity tests (S-exp set) of wind stress feedback from cyanobacteria

Experiment name	δ [m^{-3} (mmol N)$^{-1}$]	Maximum Concentration [mmol N m^{-3}]
Tau (Alb+Tau)	1.405	0.477
Tau_1/2d	0.702	0.954
Tau_1/3d	0.468	1.431
Tau_1/4d	0.351	1.907
Tau_1/5d	0.281	2.384
Tau_1/6d	0.234	2.861

climatology of CORE-II atmospheric forcing data (Large and Yeager, 2009) was used for 300-year spin up. NEMO-TOPAZ was run using CORE-II data from 1948 to 2009 with the horizontal spatial resolution of the model was $2^{o}\times2^{o}$ (182×149 grid points); data from the 29 years from 1981 to 2009 were used for performance analysis. The vertical resolution had 31 levels; the vertical thickness was 10 m from the surface to 150 m. The observational ocean temperature data used for comparison and modeling results consisted of reanalyzed data provided by the Hadley Centre of Met Office (Good et al., 2013).

2.3. Numerical Experiments

We performed two sets of model experiments in which the effects of albedo and wind stress on physical ocean environments were analyzed (F-exp set) and sensitive experiments related to the changes in wind stress due to cyanobacteria (S-exp set). The F-exp set has three runs: the albedo and wind stress changes due to phytoplankton which were not considered to the model (Control run), changes in albedo (Alb run), and changes in wind stress (Tau run). Note that Alb and Tau runs were conducted in which albedo or wind stress changes were considered

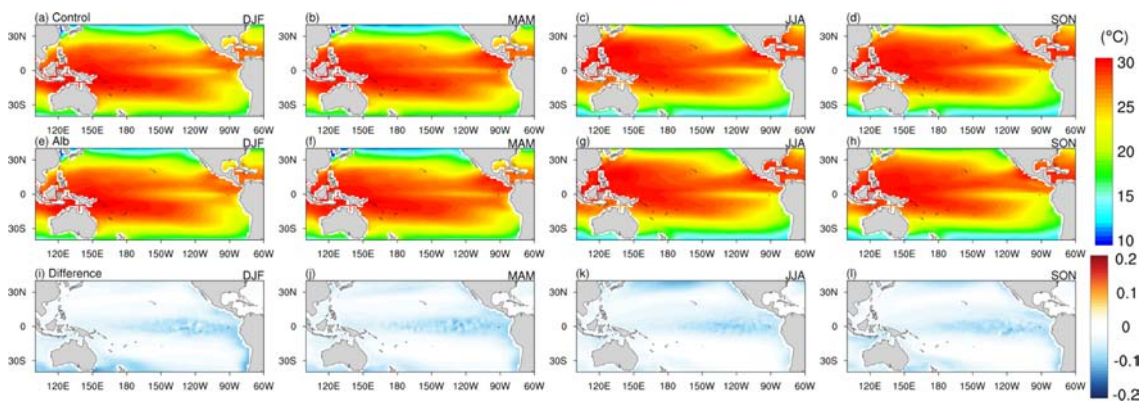

Fig. 1. Seasonal-mean SST distributions over the equatorial Pacific from 1981 to 2009. (a), (b), (c), and (d) represent the Control case, (e), (f), (g), and (h) represent the Alb case, and (i), (j), (k), and (l) represent the difference between Alb and Control runs.

separately. To investigate the combined effect, we also performed Alb+Tau run with both effects in the model. In addition, a sensitivity test was performed in which the strength of Tau effect was adjusted while applying Alb effect (S-exp set). This S-exp set was performed with manipulating δ in Equation (2) by changing the maximum concentration that can impact the physical environment through the formation of the cyanobacteria mat. Table 1 and Table 2 summarizes information for the F-exp and S-exp sets, respectively.

3. Results

3.1. Impact of the albedo and wind stress changes

Generally, an increase in the ocean surface albedo is expected to lower the upper ocean temperature by reducing the radiation transmitted to the ocean. An increase of cyanobacteria tends to enhance the ocean surface albedo (Kahru et al., 1993), causing less solar radiation to penetrate the ocean. Figure 1 shows that

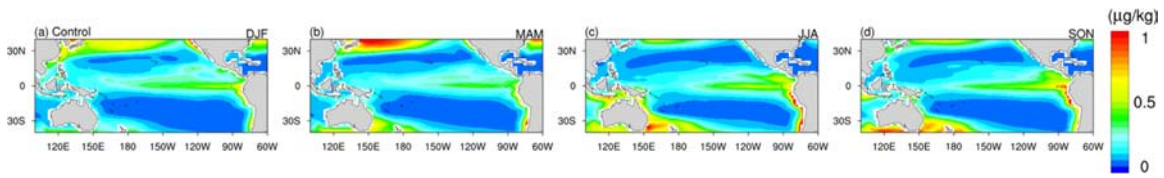

Fig. 2. Seasonal-mean surface chlorophyll distributions over the equatorial Pacific from 1981 to 2009. (a), (b), (c), and (d) present the Control run.

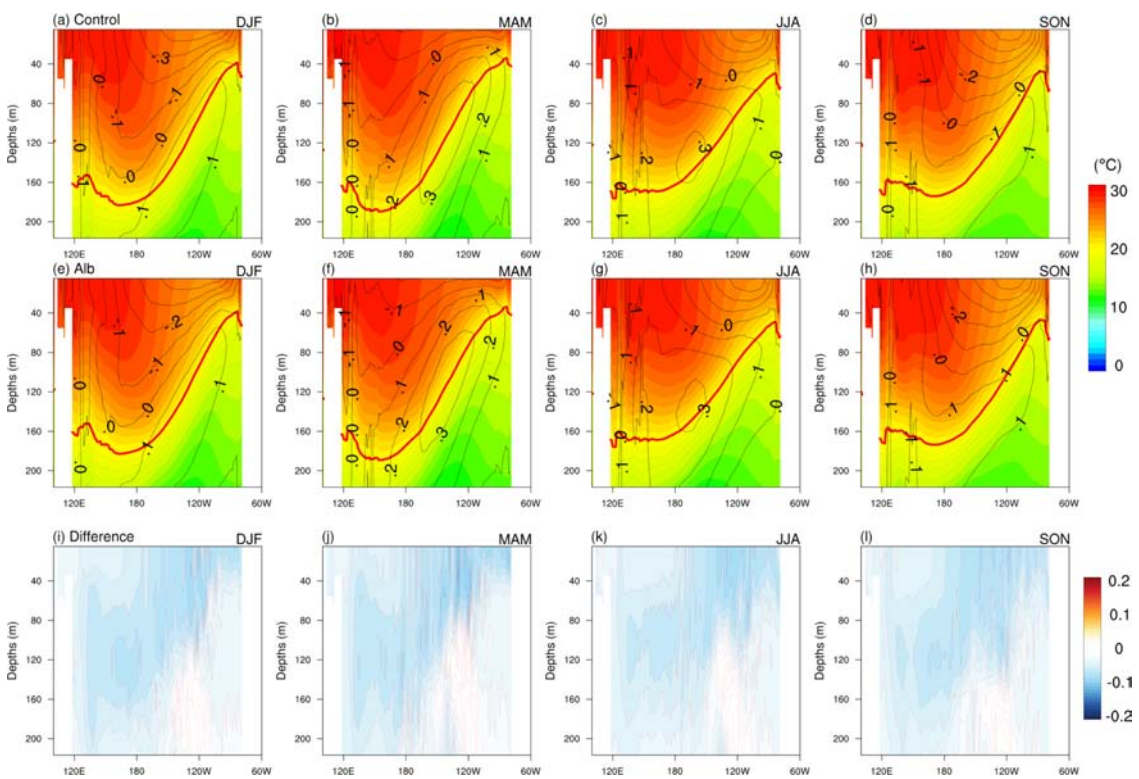

Fig. 3. Vertical distributions of the meridional-averaged (5°S-5°N) seasonal-mean temperature over the equatorial Pacific from 1981 to 2009. The contour lines indicate the zonal current (m/s). (a), (b), (c), and (d) represent the Control case, (e), (f), (g), and (h) represent the Alb case, and (i), (j), (k), and (l) represent the difference between Alb and Control runs. Red solid lines denote isothermal of 20°C.

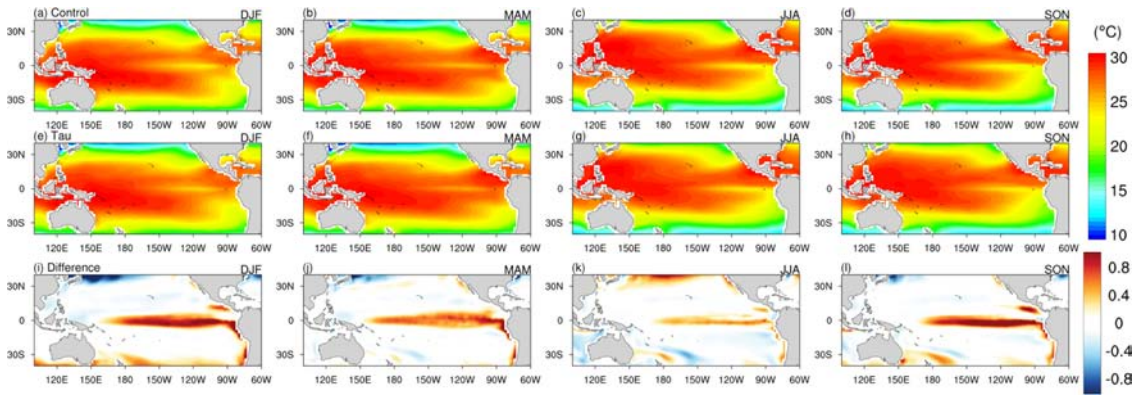

Fig. 4. Seasonal-mean SST distributions over the equatorial Pacific from 1981 to 2009. (a), (b), (c), and (d) represent the Control case, (e), (f), (g), and (h) represent the Tau case, and (i), (j), (k), and (l) represent the difference between Tau and Control runs.

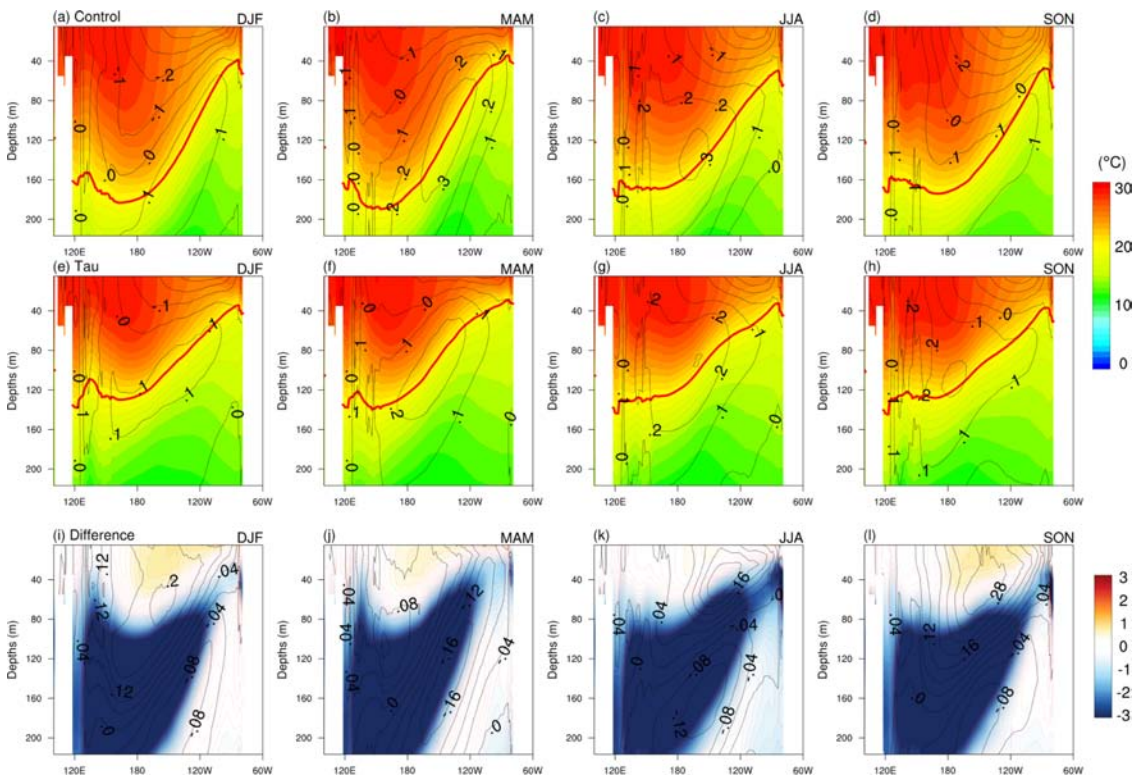

Fig. 5. Vertical distributions of the meridional-averaged (5°S-5°N) seasonal-mean temperature over the equatorial Pacific from 1981 to 2009. The contour lines indicate the zonal current (m/s). (a), (b), (c), and (d) represent the Control case, (e), (f), (g), and (h) represent the Tau case, and (i), (j), (k), and (l) represent the difference between Tau and Control runs. Red solid lines denote isothermal of 20°C.

the Alb run would have a lower sea surface temperature (SST) in the all seasons than Control run, reflecting the enhanced albedo due to cyanobacteria. Note that the regions with low SST in the Alb experiment are consistent with the distribution of phytoplankton, such as the equatorial central-eastern Pacific (Fig. 2). The vertical distribution of the ocean temperature was slightly lower in Alb than in Control, which is similar to SST (Fig. 3). However, the zonal current showed almost no difference between the two experiments.

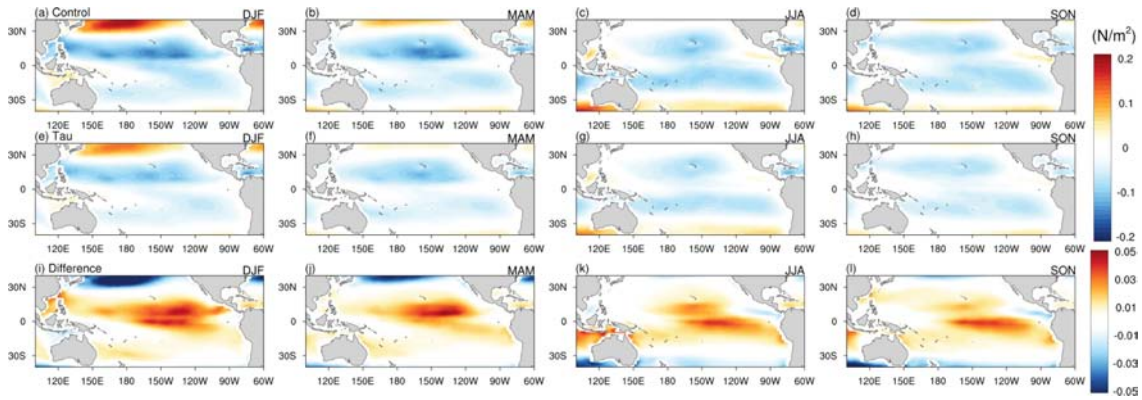

Fig. 6. Seasonal-mean zonal wind stress distributions over the equatorial Pacific from 1981 to 2009. (a), (b), (c), and (d) represent the Control case, (e), (f), (g), and (h) represent the Tau case, and (i), (j), (k), and (l) represent the difference between Tau and Control runs.

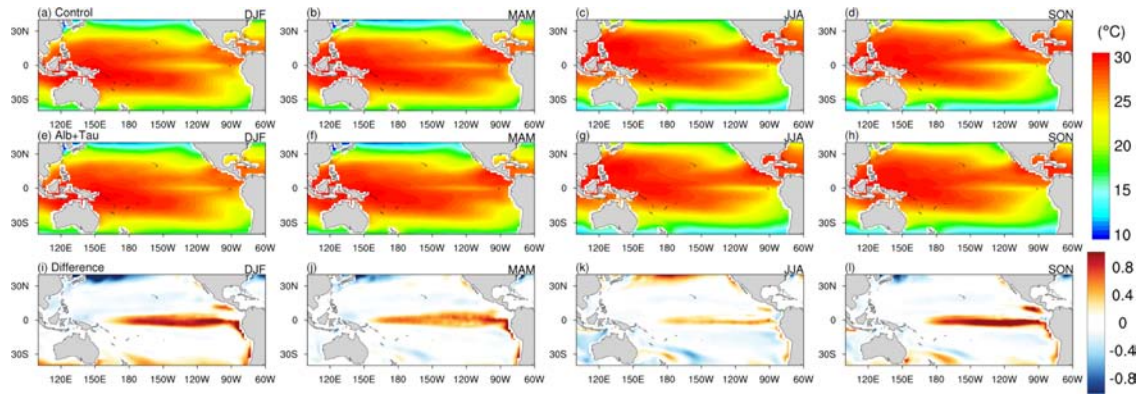

Fig. 7. Seasonal-mean SST distributions over the equatorial Pacific from 1981 to 2009. (a), (b), (c), and (d) represent the Control case, (e), (f), (g), and (h) represent the Alb+Tau case, and (i), (j), (k), and (l) represent the difference between Alb+Tau and Control runs.

Further, the effects of the changes in the ocean wind stress due to cyanobacteria, were examined. Unlike Alb run, Tau run simulated the SST of the equatorial region to be higher than that of Control (Fig. 4). The SST difference of Tau was higher than of Alb, indicating that the impact of the biological changes in wind stress was greater than that of albedo. The regions with the SST of Tau being higher than that of Control were consistent with the distribution of phytoplankton (Fig. 2). To determine why SST is higher in Tau experiment, the vertical ocean temperature was analyzed, as well as the zonal current and zonal wind stress. Figure 5 presents the vertical ocean temperature distribution and zonal current of Control and Tau runs in the equatorial Pacific. These results confirm that Tau run estimated a shallower equatorial thermocline depth than Control run. Based on the differences between the two experiments, it was determined that Tau showed higher ocean temperatures than Control at depths above 40 m during DJF, MAM, and SON seasons, along with a reduction in the easterly current for a same depth (Fig. 5i, j, and l). Such phenomena could be explained with a zonal wind stress analysis. With respect to the differences in the zonal wind stress of Tau run, a westerly current appeared due to the decrease in the influence of trade winds as compared to Control run (Fig. 6i, j, k, and l). Therefore, the upwelling in the eastern Pacific became weaker, which resulted in an increase in SST and reduction in the zonal thermocline slope, as

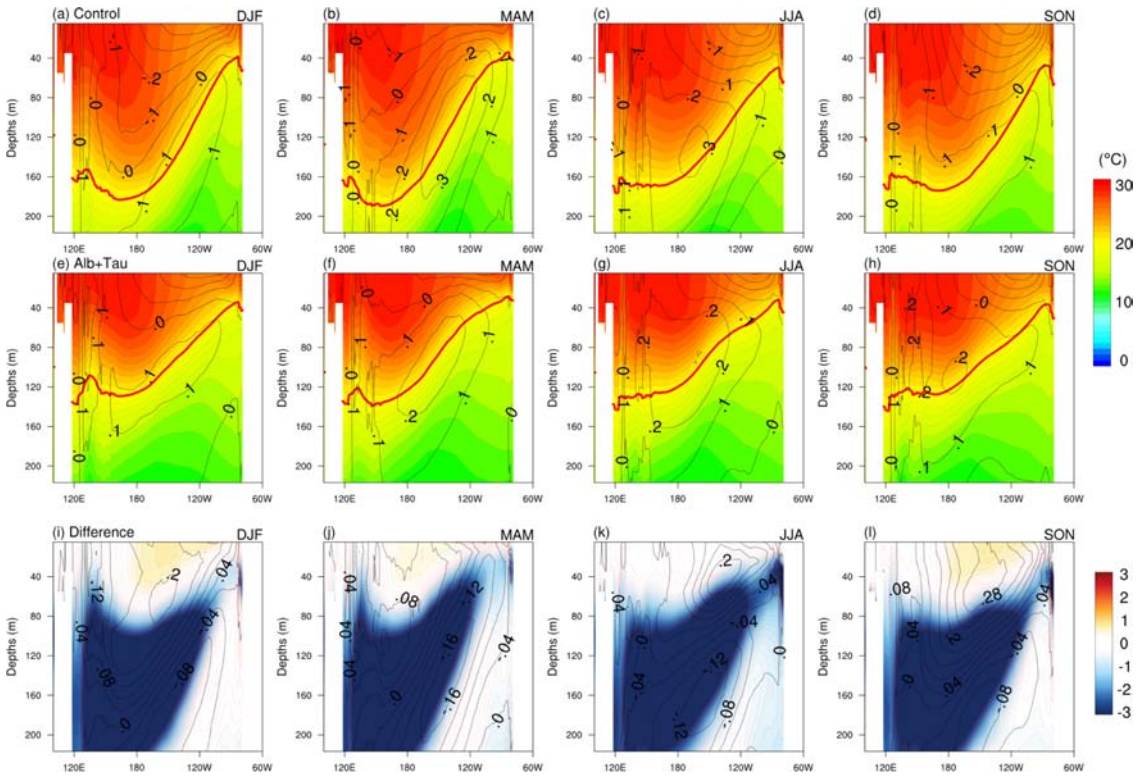

Fig. 8. Vertical distributions of the meridional-averaged (5°S-5°N) seasonal-mean temperature over the equatorial Pacific from 1981 to 2009. The contour lines indicate zonal current (m/s). (a), (b), (c), and (d) represent the Control case, (e), (f), (g), and (h) represent the Alb+Tau case, (i), (j), (k), and (l) represent the difference between Alb+Tau and Control runs. Red solid lines denote isothermal of 20°C.

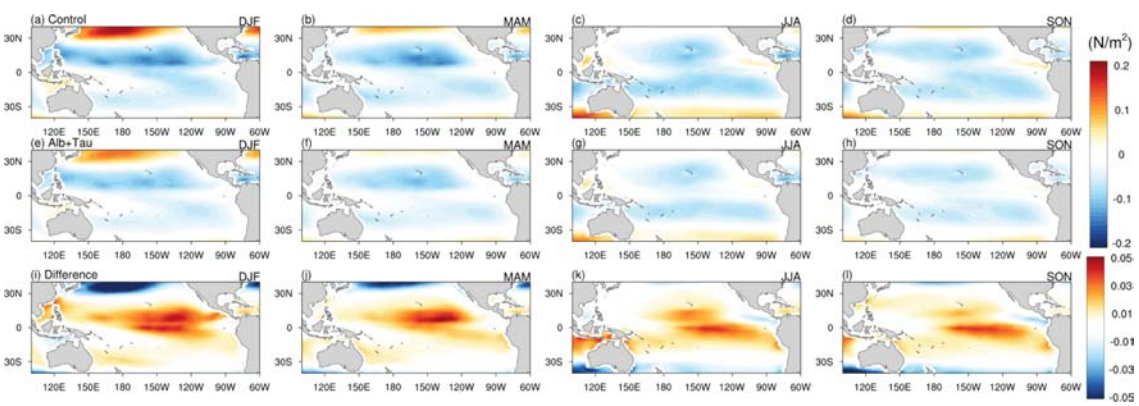

Fig. 9. Seasonal-mean zonal wind stress distributions over the equatorial Pacific from 1981 to 2009. (a), (b), (c), and (d) represent the Control case, (e), (f), (g), and (h) represent the Alb+Tau case, and (i), (j), (k), and (l) represent the difference between Alb+Tau and Control runs.

shown in Fig. 4 and 5. The differences in SST were greater during the DJF and SON seasons because the SST is affected by the weakened trade winds due to the cyanobacteria during the ENSO mature season (Fig. 4).

As observed in the comparative analysis between Alb and Control runs, the impact of the albedo changes was relatively weaker than that of the wind

stress. Accordingly, the Alb+Tau results were similar to Tau results. Alb+Tau also simulated the eastern equatorial thermocline depth to be shallower than Control run, showing a pattern associated with a weakened influence of the trade winds, such as an elevated SST in the equatorial Pacific (Fig. 7-9).

Figure 10 shows the biases of the monthly-mean SST in Niño regions 3, 3.4, and 4. It appeared that the model generally underestimated the equatorial SST as shown in Control run. When the biological change in albedo was applied, the negative bias increased slightly in all regions (Alb run). However, the Tau run shows the positive biases, whose magnitudes seem to be higher than other experiments during ENSO mature season. Because upwelling occurred in the Niño 3 region having a higher phytoplankton concentration than other regions, the wind stress exerts the most important influence on SST (Fig. 10a). The Niño 4 region presented a weak seasonal impact (Fig. 10c). The positive bias was large during the DJF and SON seasons, as it corresponds to ENSO peak seasons and mass proliferation of phytoplankton, such as cyanobacteria. Moreover, considering that the positive biases of the SST due to the altered wind stress were overestimated in all Niño regions, this effect should be adjusted to weaken in the model. Herein, the parameter in the feedback equation was manipulated in the sensitivity tests (S-exp set) and the results will be discussed in a subsequent section.

In addition, the monthly variability of the SST and Niño index over 29 years was also examined (Fig. 11 and 12). It can be observed that the impact of albedo was weaker than that of wind stress (Fig. 12). However, as shown in Fig. 12, the altered albedo increased the biases of the standard deviation (SD) for all months in all regions. When the wind stress changes due to phytoplankton was applied, the biases of the SD of the SST decreased significantly. In particular, the results show these decreases even further during the ENSO peak seasons (Fig. 12). While the model overestimated the variability in ENSO and equatorial Pacific SST (the bias of SD of the equatorial Pacific SST is +0.28°C), it is believed

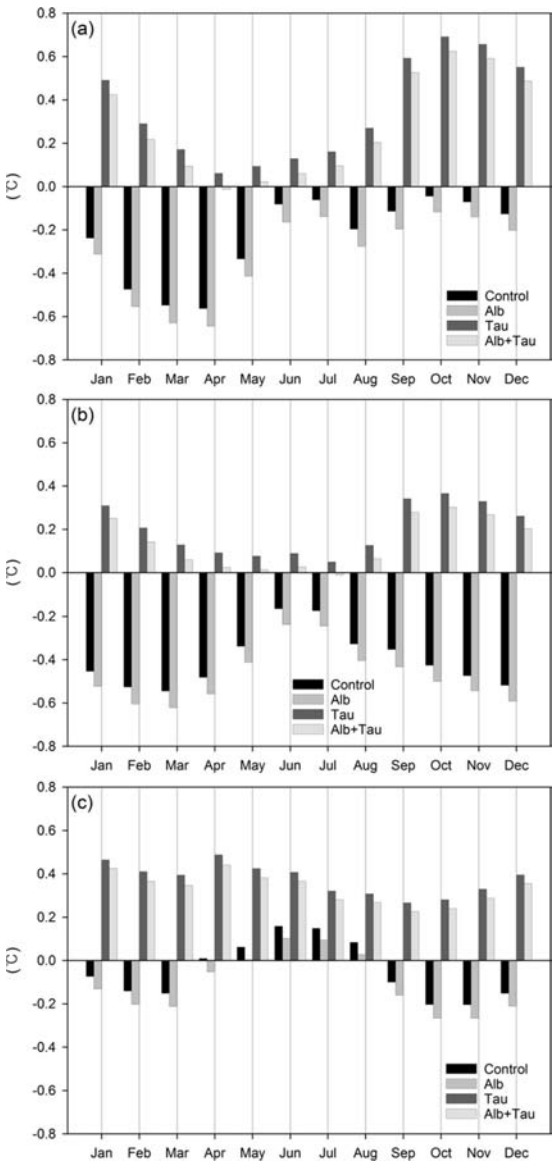

Fig. 10. Biases of monthly-mean SST over the (a) Niño 3, (b) Niño 3.4, and (c) Niño 4 regions from 1981 to 2009.

that the bias of SD of SST could be reduced to +0.13°C by applying the biological wind stress effect.

3.2. Sensitivity test of wind stress effect

As described above, the top 25% average values of small cyanobacteria concentrations simulated by NEMO-TOPAZ model for a 62-year period were used to determine the maximum concentration. However, as shown in Fig. 10, the Tau run shows increases in

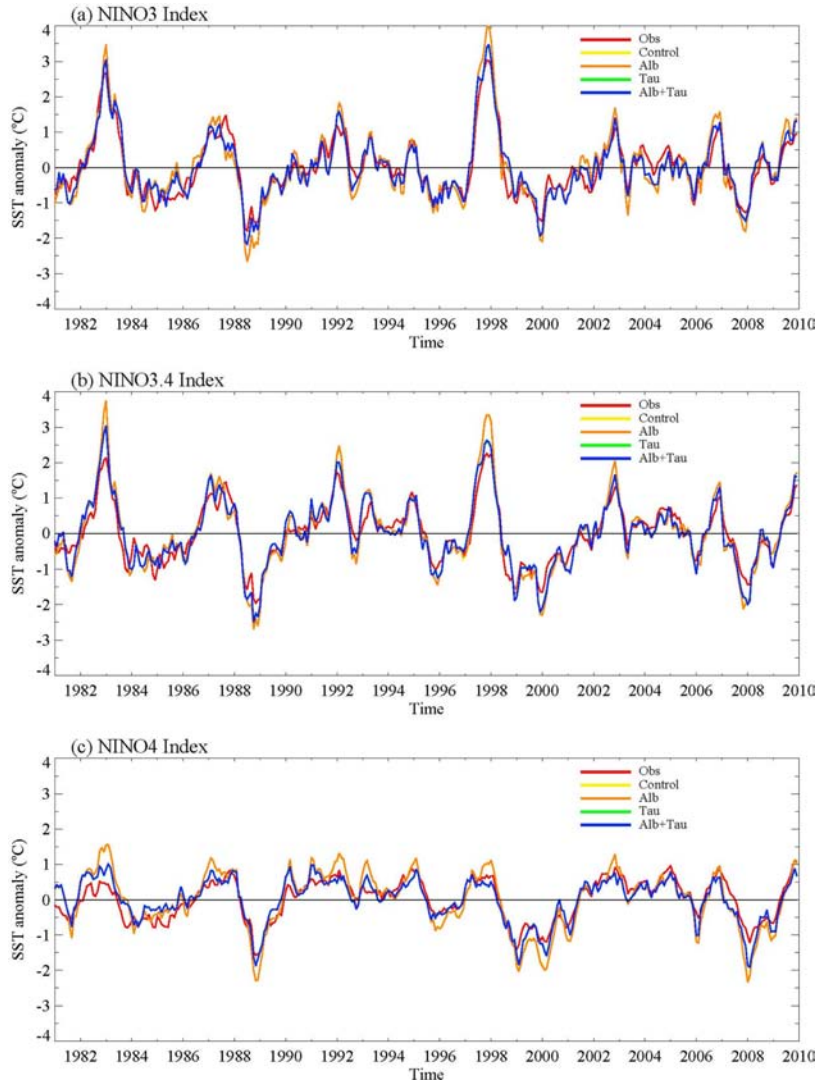

Fig. 11. Time series of (a) Niño 3, (b) Niño 3.4, and (c) Niño 4 indices from 1981 to 2009.

biases of the monthly SST in Niño regions. Therefore, the maximum concentration and δ in Equation (2) were manipulated to investigate the changes in the equatorial Pacific SST according to the strength of the biological effects, as shown in Table 2. Tau_1/6d represents the model experiment in which δ was divided by 6 as compared to Tau run, correspondingly, the impact of the wind stress would also be reduced.

The seasonal SSTs show increases in the negative biases in the central Pacific with decreasing impact of wind stress, especially in the DJF and SON seasons (Fig. 13). However, the positive bias appearing in the northern and southern regions of the equatorial eastern Pacific decreased (Fig. 13). Similar features were also found in the monthly SST (Fig. 14). These results are attributed to an underestimation of the equatorial SST of the model, relative to the observation, and thus, the original error was reduced as the impact of the biological wind stress decreased. In terms of RMSE of the seasonal SST in Niño regions, Tau_1/2d run presents the lowest errors (Table 3). According to the SD of the equatorial Pacific SST, the bias of the SST variability increased as the wind stress effect became weaker in all Niño regions (Fig. 15).

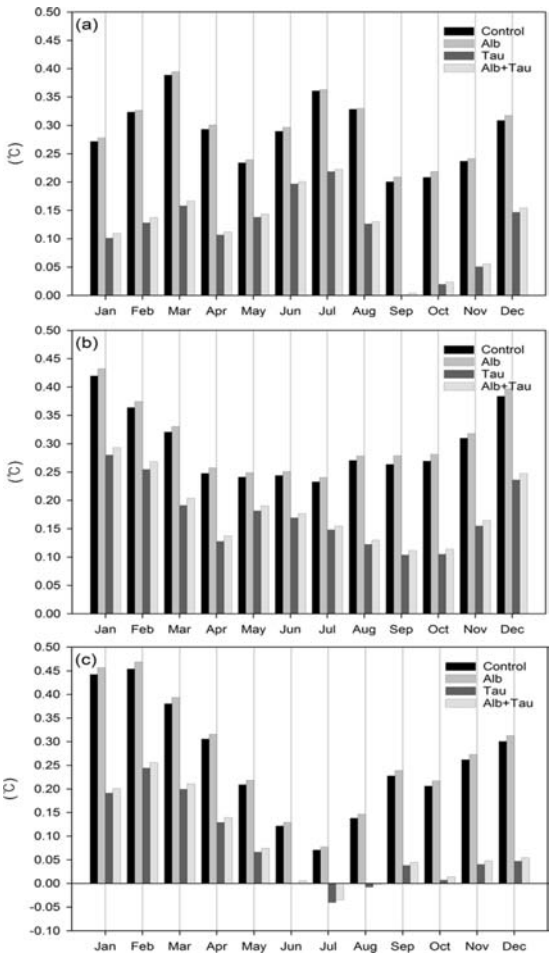

Fig. 12. Biases of standard deviation of monthly-mean SST over the (a) Niño 3, (b) Niño 3.4, and (c) Niño 4 regions from 1981 to 2009.

The biological modulation of wind stress can affect the strength of upwelling by weakening the impact of trade winds in the present of phytoplankton. Here, the vertical ocean temperature distribution in the equatorial Pacific region was examined for each sensitivity case. NEMO-TOPAZ simulated a thermocline depth (slope) deeper (larger) than observation (Fig. 16). This is consistent with the fact that the model overestimates the variability of the equatorial Pacific SST, namely the ENSO amplitude, as compared to observation (Fig. 11 and 12). However, as the altered wind stress was applied, its impact became weaker, the model shows that the thermocline depth and slope is similar to the observation (Fig. 16). The RMSE of the vertical temperature in the equatorial Pacific supports these results (Table 4).

4. Summary and Discussion

The present study applied the biological effects associated with wind stress and surface albedo due to small cyanobacteria to NEMO-TOPAZ, a newly developed coupled global ocean-biogeochemistry model and investigate the variability of SST in the equatorial Pacific. The altered albedo due to cyanobacteria decreased the SST in the equatorial Pacific, but its impact was found to be smaller than that of wind stress. The cyanobacteria decreased the wind stress forcing associated with trade winds and weakened upwelling, and as a result, the equatorial SST increased. The Control experiment overestimated the variability of ENSO, but this bias was reduced by biological changes in wind stress.

We also examined the impact of wind stress on the equatorial Pacific through sensitivity tests with tuned parameter values. Here a simple form of feedback equations determined by Sonntag (2013) was used. However, simple equations may not be able to accurately express the rate of change in wind stress and albedo due to cyanobacteria in nature. Therefore, to complete the feedback scheme of phytoplankton in the model, a mathematical study based on careful observations is required. At the same time, future work on converting observation-based equations and coefficients that can be applied to low-resolution climate models is necessary. Such studies may reduce misfits between observations and climate models.

Here we focus the biological effects of wind stress and albedo due to cyanobacteria on the equatorial Pacific region. However, phytoplankton, such as cyanobacteria, is abundantly found according to seasonal variability in not only the middle latitudes, but in the polar regions as well. Therefore, further studies on middle latitude and the polar oceans would be necessary. Finally, we used an ocean model forced by fixed atmospheric fields. In reality, however, changes in ocean temperature can lead to atmospheric changes

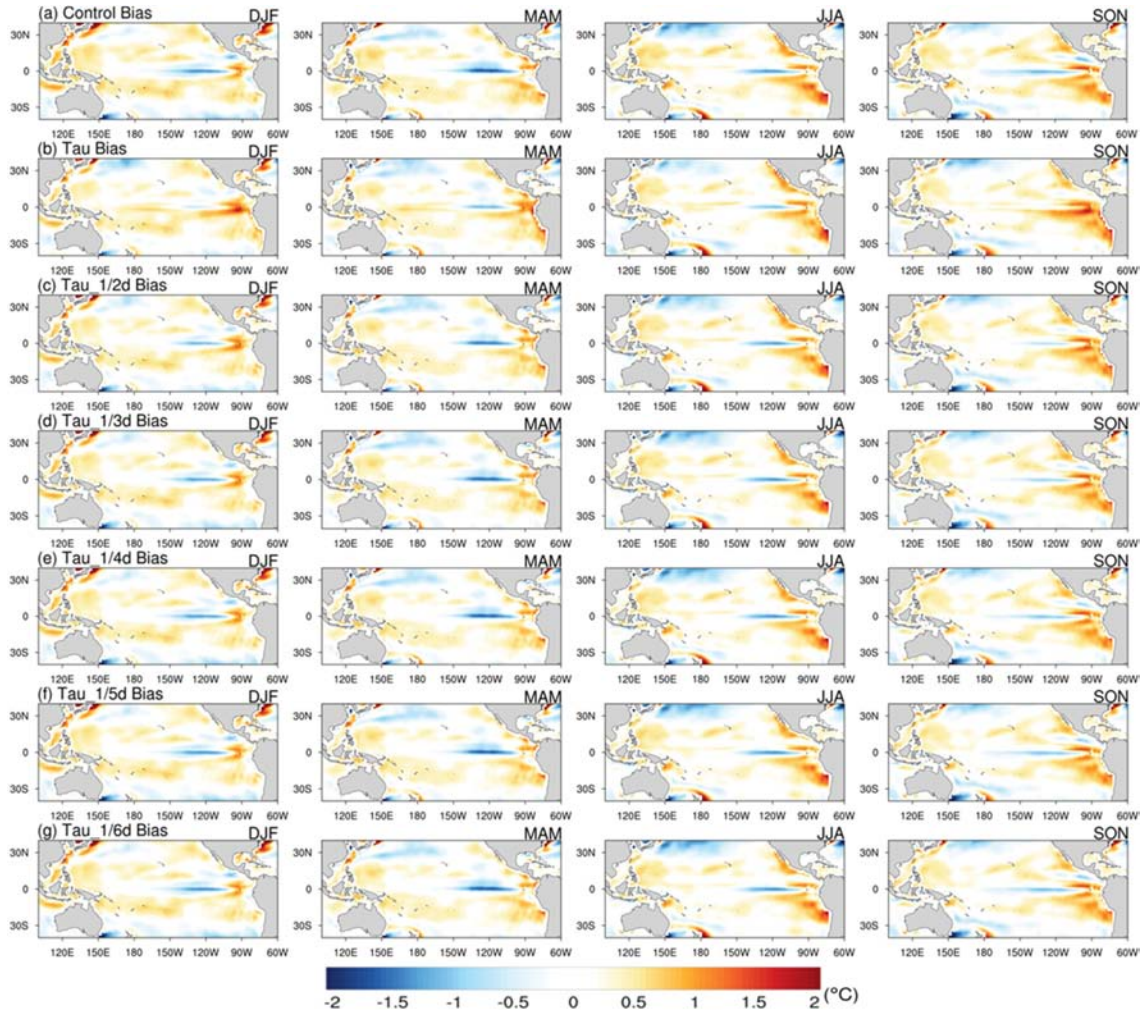

Fig. 13. Biases of the seasonal-mean SST over the equatorial Pacific from 1981 to 2009 in each sensitivity test, as seen in Table 2.

via air-sea interactions (e.g., Hense et al., 2017). Thus, the air-sea coupled interactions together with biophysical feedbacks should be considered using fully-coupled atmosphere-ocean climate models.

Acknowledgments

The main calculations were performed by using the supercomputing resource of the Korea Meteorological Administration (National Center for Meteorological Supercomputer). This work is a park of Dr. Jung's Ph.D. thesis.

References

ARCCSS, 2018, MOM5 input data, Australian Research Council's Centre of Excellence for Climate System Science. http://climate-cms.unsw.wikispaces.net/Data. Accessed 22 November 2018 (note: resource no longer exists online).

Arrigo, K.R., Robinson, D.H., Worthen, D.L., Dunbar, R.B., DiTullio, G.R., VanWoert, M., and Lizotte, M.P., 1999, Phytoplankton community structure and the drawdown of nutrients and co2 in the Southern Ocean. Science, 283, 365-367.

Burchard, H., Bolding, K., Kuhn, W., Meister, A., Neumann, T., and Umlauf, L., 2006, Description of a

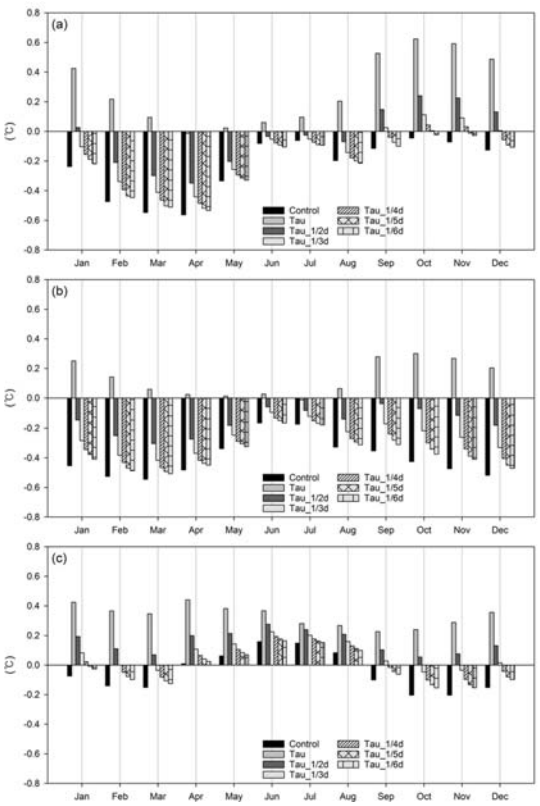

Fig. 14. Biases of the monthly-mean SST over the (a) Niño 3, (b) Niño 3.4, and (c) Niño 4 regions from 1981 to 2009 in each sensitivity test, as seen in Table 2.

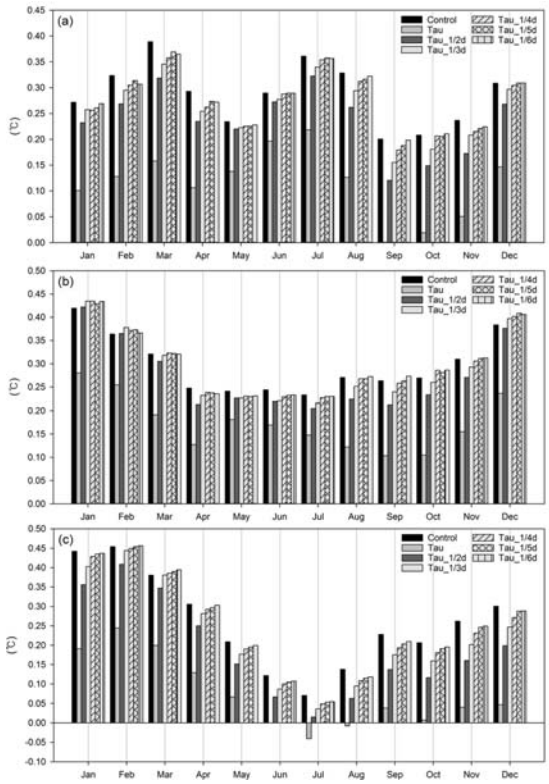

Fig. 15. Biases of standard deviation of monthly-mean SST over the (a) Niño 3, (b) Niño 3.4, and (c) Niño 4 regions from 1981 to 2009 in each sensitivity test, as seen in Table 2.

flexible and extendable physical-biogeochemical model system for the water column, Journal of Marine Systems, 61, 180-211, doi:10.1016/j.jmarsys.2005.04.011.

Deacon, E.L., 1979, The role of coral mucus in reducing the wind drag over coral reefs, Boundary-Layer Meteorology, 17(4), 517-521, doi:10.1007/BF00118614.

Dunne, J.P., John, J.G., Shevliakova, E., Stouffer, R.J., Krasting, J.P., Malyshev, S.L., Milly, P.C.D, Sentman, L.T., Adcroft, A.J., Cooke, W., Dunne, K.A., Griffies, S.M., Hallberg, R.W., Harrison, M.J., Levy, H., Wittenberg, A.T., Phillips, P.J., and Zadeh, N., 2012, GFDL's ESM2 global coupled climate-carbon earth system models. Part II: carbon system formulation and baseline simulation characteristics, Journal of Climate, 26, 2247-2267, doi:10.1175/jcli-d-12-00150.1.

Good, S.A., Martin, M.J., and Rayner, N.A., 2013, EN4: Quality controlled ocean temperature and salinity profiles and monthly objective analyses with uncertainty estimates, Journal of Geophysical Research-Oceans, 118, 6704-6716, doi:10.1002/2013JC009067.

Hense, I., Stemmler, I., and Sonntag, S., 2017, Ideas and

Table 3. RMSE of seasonal SST (^{o}C) over the equatorial Pacific (160^{o}E-90^{o}W, 5^{o}S-5^{o}N)

	DJF	MAM	JJA	SON	Average
Control	0.551	0.600	0.508	0.553	0.553
Tau (Alb+Tau)	0.571	0.513	0.492	0.595	0.543
Tau_1/2d	0.483	0.524	0.499	0.461	0.492
Tau_1/3d	0.502	0.549	0.504	0.471	0.506
Tau_1/4d	0.515	0.566	0.507	0.492	0.520
Tau_1/5d	0.530	0.579	0.510	0.507	0.532
Tau_1/6d	0.538	0.585	0.512	0.519	0.538

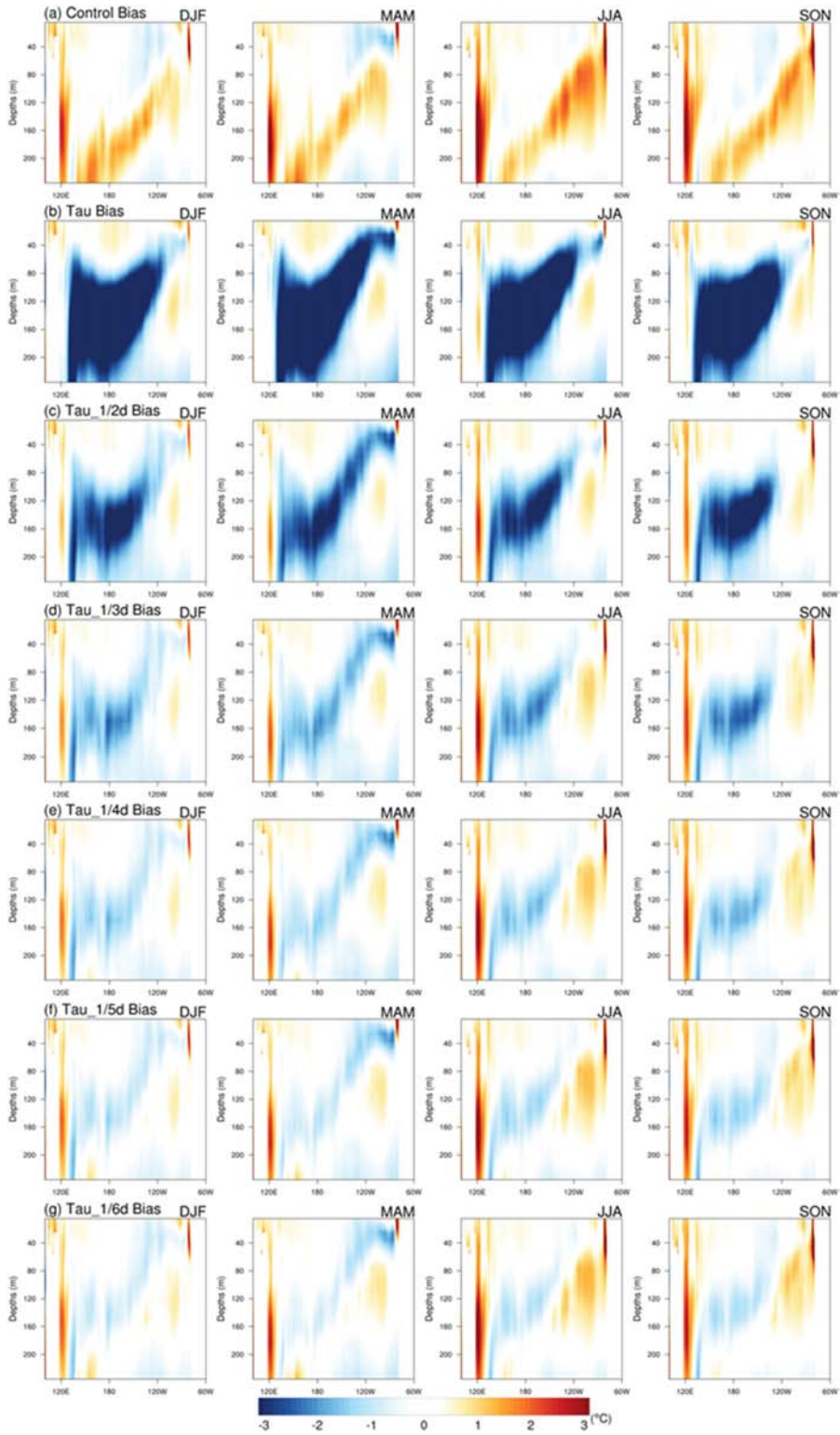

Fig. 16. Vertical distributions of the meridional-averaged (5°S-5°N) seasonal-mean temperature over the equatorial Pacific from 1981 to 2009 in each sensitivity test, as seen in Table 2.

Table 4. RMSE of seasonal vertical temperature (surface to 250 m) (^{o}C) over the equatorial Pacific (160^{o}E-90^{o}W, 5^{o}S-5^{o}N)

	DJF	MAM	JJA	SON	Average
Control	0.721	0.761	0.971	0.930	0.846
Tau (Alb+Tau)	2.651	2.609	2.483	2.596	2.582
Tau_1/2d	1.310	1.319	1.265	1.351	1.311
Tau_1/3d	0.860	0.899	0.915	0.964	0.910
Tau_1/4d	0.691	0.746	0.815	0.835	0.772
Tau_1/5d	0.623	0.685	0.788	0.792	0.722
Tau_1/6d	0.598	0.660	0.787	0.781	0.707

perspectives: Climate-relevant marine biologically driven mechanisms in earth system models. Biogeosciences, 14, 403-413, doi:10.5194/bg-14-403-2017.

Hutchinson, P.A., and Webster, I.T., 1994, On the distribution of bluegreen algae in lakes: Wind-tunnel tank experiments, Limnology and Oceanography, 39(2), 374-382.

Jung, H.-C., 2019, Development and assessment of a coupled ocean-biogeochemistry model. Unpublished Ph.D. dissertation, Chonbuk National University, Jeonju, Korea, 164p.

Kahru, M., Leppänen, J., and Rud, O., 1993, Cyano-bacterial blooms cause heating of the sea surface, Marine Ecology Progress Series, 101, 1-7.

Large, W.G. and Yeager, S.G., 2009, The global climatology of an interannually varying air-sea flux data set, Climate Dynamics, 33, 341-364, doi:10.1007/s00382-008-0441-3.

LaRoche, J. and Breitbarth, E., 2005, Importance of the diazotrophs as a source of new nitrogen in the ocean. Journal of Sea Research, 53, 67-91, doi:10.1016/j.seares.2004.05.005.

Lim, H.-G., Park, J.-Y., and Kug, J.-S., 2017, Impact of chlorophyll bias on the tropical Pacific mean climate in an earth system model, Climate Dynamics, doi:10.1007/s00382-017-4036-8.

Park, H.-J., Moon, B.-K., Wie, J., Kim, K.-Y., Lee, J., Byun, Y.-H., 2017, Biophysical Effects Simulated by an Ocean General Circulation Model Coupled with a Biogeochemical Model in the Tropical Pacific, Journal of Korean Earth Science Society, 38(7), 469-480, http://doi.org/10.5467/JKESS.2017.38.7.469.

Park, J.-Y., Dunne, J.P., and Stock, C.A., 2018, Ocean chlorophyll as a precursor of ENSO: An Earth system modeling study, Geophysical Research Letters, 45, 1939-1947, doi:10.1002/2017GL076077.

Park, J.-Y., Kug, J.-S., Bader, J., Rolph R., and Kwon M., 2015, Amplified Arctic warming by phytoplankton under greenhouse warming, Proceedings of the National Academy of Sciences of the United States of America, 112, 5921-5926, doi:10.1073/pnas.1416884112.

Park, J.-Y., Kug, J.-S., Park, J.-S., Yeh, S.-W., and Jang, C.J., 2011, Variability of chlorophyll associated with ENSO and its possible biological feedback in the Equatorial Pacific, Journal of Geophysical Research, 116, C10001, https://doi:10.1029/2011JC007056.

Park, J.-Y., Kug, J.-S., Seo, H., and Bader J., 2014, Impact of bio-physical feedbacks on the tropical climate in coupled and uncoupled GCMs, Climate Dynamics, 43, 1811-1827, https://doi:10.1007/s00382-013-2009-0.

Park, J.-Y., Stock, C.A., Dunne, J.P., Yang, X.S., and Rosati, A., 2019, Seasonal to multiannual marine ecosystem prediction with a global earth system model. Science, 365, 284-288.

Sathyendranath, S., Gouveia, A.D., Shetye, S.R., Ravindran, P., and Platt, T., 1991, Biological control of surface temperature in the Arabian Sea, Nature, 349(6304), 54-56, doi:10.1038/349054a0.

Sonntag, S., 2013, Modeling biological-physical feedback mechanisms in marine system (Doctoral dissertation), University of Hamburg, Germany.

Sonntag, S., and Hense, I., 2011, Phytoplankton behavior affects ocean mixed layer dynamics through biological-physical feedback mechanisms, Geophysical Research Letters, 38, L15610, doi:10.1029/2011GL048205.

Stal, L.J., 2009, Is the distribution of nitrogen-fixing cyanobacteria in the oceans related to temperature? Environmental Microbiology, 11, 1632-1645, doi:10.1111/j.1758-2229.2009.00016.x.

Manuscript received: July 30, 2019
Revised manuscript received: August 15, 2019
Manuscript accepted: August 23, 2019